



# DLK-MAPK Signaling Coupled with DNA Damage Promotes Intrinsic Neurotoxicity Associated with Non-Mutated Tau

Sanming Li<sup>1</sup> · Ethan R. Roy<sup>1</sup> · Yanyu Wang<sup>1</sup> · Trent Watkins<sup>2</sup> · Wei Cao<sup>1</sup>

Received: 28 April 2023 / Accepted: 17 October 2023 / Published online: 13 November 2023  
© The Author(s) 2023

## Abstract

Alzheimer's disease (AD) is the most prevalent form of neurodegeneration. Despite the well-established link between tau aggregation and clinical progression, the major pathways driven by this protein to intrinsically damage neurons are incompletely understood. To model AD-relevant neurodegeneration driven by tau, we overexpressed non-mutated human tau in primary mouse neurons and observed substantial axonal degeneration and cell death, a process accompanied by activated caspase 3. Mechanistically, we detected deformation of the nuclear envelope and increased DNA damage response in tau-expressing neurons. Gene profiling analysis further revealed significant alterations in the mitogen-activated protein kinase (MAPK) pathway; moreover, inhibitors of dual leucine zipper kinase (DLK) and c-Jun N-terminal kinase (JNK) were effective in alleviating wild-type human tau-induced neurodegeneration. In contrast, mutant P301L human tau was less toxic to neurons, despite causing comparable DNA damage. Axonal DLK activation induced by wild-type tau potentiated the impact of DNA damage response, resulting in overt neurotoxicity. In summary, we have established a cellular tauopathy model highly relevant to AD and identified a functional synergy between the DLK-MAPK axis and DNA damage response in the neuronal degenerative process.

**Keywords** Alzheimer · Tauopathy · Neurodegeneration · DNA damage · MAP kinase · DLK · Axonal degeneration

## Abbreviations

AAV	Adeno-associated virus	MAP3K	MAP kinase kinase kinase
AD	Alzheimer's disease	MAPK	Mitogen-activated protein kinase
AP-1	Activator protein 1	MAPT	Microtubule associated protein tau
CBD	Corticobasal degeneration	NFT	Neurofibrillary tangles
CNS	Central nervous system	p-c-Jun	Phospho-c-Jun
DDR	DNA damage response	pH2AX	Phospho-Histone H2A.X
DLK	Dual leucine zipper kinase	p-JNK	Phospho-JNK
DLKi	DLK inhibitor	pNF-H	Phospho-Neurofilament H
dsDNA	Double stranded DNA	p-p53	Phospho-p53
FTLD	Frontotemporal lobar degeneration	PSP	Progressive supranuclear palsy
hTau	Human tau	RNAseq	RNA Sequencing
JNK	c-Jun N-terminal kinase	SYN1	Synapsin I
JNKi	JNK inhibitor	ThioS	Thioflavin S
LDH	Lactate dehydrogenase	WT	Wild-type
		Z-VAD	Z-VAD-FMK

✉ Wei Cao  
wei.cao@uth.tmc.edu

<sup>1</sup> Department of Anesthesiology, Critical Care and Pain Medicine, McGovern Medical School, University of Texas Health Science Center at Houston, Houston, TX 77030, USA

<sup>2</sup> Present Address: Department of Neurology, University of California, San Francisco, CA 94158, USA

## Introduction

Microtubule-associated protein tau (encoded by *MAPT* gene) is centrally involved in the pathogenesis of Alzheimer's disease (AD) and a group of neurodegenerative disorders coined as “tauopathies”, which display a hallmark

of excessive tau aggregation in the brain [1–3]. Tau is most abundantly expressed in neurons, where it primarily associates with and stabilizes microtubules. Besides this role, tau has been shown to fulfill biological functions in regulating key neuronal processes, including axonal transport, cytoskeletal dynamics, synaptic transmission, nuclear transport, protein translation, mitochondrial function, and metabolism [4–7]. The complex biology of this intrinsically disordered protein entails multiple isoforms generated from alternative splicing of a single *MAPT* gene, a plethora of post-translational modifications at various sites of the protein, and the discrete roles played by tau in different cellular compartments [8–12].

AD distinguishes from other tauopathies by presentation as a secondary tauopathy. In primary tauopathy conditions, such as frontotemporal lobar degeneration (FTLD), Pick disease, progressive supranuclear palsy (PSP), corticobasal degeneration (CBD), and chronic traumatic encephalopathy (CTE), a large number of rare *MAPT* mutations predispose the development of tau pathology in the central nervous system (CNS)<sup>10</sup>. In contrast, the vast majority of AD patients possess non-mutated *MAPT* while developing abundant amyloid plaques in conjunction with neurofibrillary tangles (NFT) that contain insoluble tau aggregates in their brains [6, 7]. Through studying animal and cell culture models expressing mutated *MAPT*, many groups over the years have elucidated the pathogenic potential of FTLD-associated mutant tau [13–17]. However, a critical question that remains to date is whether the pathogenic role of tau in AD is in any way dissimilar from that in primary tauopathy. If so, the findings from the mutant tau studies might be inadequate to guide the therapeutic development for AD.

Elevated tau protein level is causally linked to disease pathogenesis; in particular, intraneuronal accumulation of aggregated tau closely correlates with the clinical progression of AD as well as other tauopathies [18, 19]. In rodent brains, neuronal overexpression of mutant *MAPT* is sufficient for the development of NFT pathology and the onset of neurodegeneration, leading to the successful construction of numerous tauopathy disease models [14, 16]. *In vitro*, however, tau overexpression has been mostly carried out in immortalized non-neuronal cells, such as HEK293 and HELA cells, to facilitate studies on the tau interactome, transcriptomic influence by tau, or self-aggregation and seeding properties of tau [20–22]. Neuronal cell lines and human induced pluripotent stem cells have also been used to study the effects of elevated tau [23, 24]. Surprisingly little is known about the functional impact of increased intraneuronal tau on differentiated primary neurons. Consequently, the major cellular pathways that govern tau-mediated neuropathology relevant to AD remain poorly understood.

To investigate AD-relevant tau-dependent neurodegeneration, we developed a cellular tauopathy model by overexpressing human tau in mouse primary neurons. This system afforded us to comprehensively assess neuronal intrinsic responses to full-length wild-type (WT) tau, and enabled a direct comparison with an FTLD-associated mutant form. Remarkably, we have detected heightened neurotoxicity triggered by WT tau and obtained insights on two major signaling pathways that promote the degenerative process that is pertinent to AD.

## Materials and Methods

### Animals

C57BL/6J mice bred from line originally obtained from the Jackson Laboratory were used in this study. Mice were housed in groups of 2–3 per cage under conventional or specific pathogen-free conditions and standard light/dark cycle. Both male and female neonates were used in experiments. All animal procedures were performed in accordance with NIH guidelines. The experimental protocols were approved by the Animal Welfare Committee of The University of Texas Health Science Center at Houston (Protocol number: AWC-22-0011) or Institutional Animal Care and Use Committee of Baylor College of Medicine (Protocol number: AN-8203).

### Generation of AAV Vectors

Recombinant AAV1/2 vectors containing the longest tau isoform (2N4R) of human *MAPT* cDNA of wild-type and mutant P301L under human SYN1 promoter were used [25]. To construct a control vector, a stop codon arisen from single nucleotide mutation was generated at the N-terminus of the *MAPT* sequence. The detailed sequences were provided in supplemental data 4. Recombinant AAV stocks were produced by Gene Vector Core at Baylor College of Medicine. Vector genomes were titrated by quantitative PCR and purity validated by SDS-PAGE. The titer of  $4 \times 10^9$  GC/ml was selected for neuronal cell infection.

### Primary Cultures of Mouse Cortical and Hippocampal Neurons

Primary neurons were harvested and cultured as previously described [26]. Briefly, P0 pups of mixed sexes were decapitated into ice-cold dissection buffer (1x HBSS supplemented with 10 mM HEPES, pH 7.5, 0.6% glucose, 20 U/ml penicillin, 20 µg/ml streptomycin).

Forebrain hemispheres were dissected and stripped of meninges. The tissues of cortex with hippocampus were isolated using a dissecting microscope and digested in trypsin at 37 °C for 15 minutes with gentle swirling. Following addition of 500 µl trypsin (2.5%), 400 µl soybean trypsin inhibitor (1 mg/ml) and 100 µl DNase I (1%) were then added. After tissue pieces decanted off, the supernatant was removed and replaced with 2 ml of DMEM and 20 µl DNase I (1%). The digested tissues were triturated with a P1000 pipette tip 8–10 times. After allowing the remaining pieces to settle, the supernatant was collected into a fresh tube for centrifuging at 1200 rpm for 5 min. The cell pellet was resuspended with 5 ml of DMEM and then centrifuged again. After carefully removed the supernatant, the dissociated cells were resuspended in 2 ml completed neuronal culture media (Neurobasal medium supplemented with 2% B27, 0.5 mM L-glutamine, 40 U/ml penicillin, 40 µg/ml streptomycin), and passed through a 70 µm filter. The single suspended cells were plated into poly D-lysine-coated culture plates or glass coverslips (1–2 × 10<sup>5</sup> cells/cm<sup>2</sup>). Cells were maintained in incubators at 37 °C, 5% CO<sub>2</sub>, and half the culture medium was replaced every 5–7 days.

### LDH Cytotoxicity Assay

50 µl of culture media was analyzed by the standard procedure provided by the manufacturer (Cat# C20301, CyQUANT™ LDH Cytotoxicity Assay, ThermoFisher, USA). The absorbance by excitation of 560 nm and emission of 590 nm was measured on the SpectraMax® ABS Microplate Reader (Molecular Devices, USA).

### Neuronal Culture Treatments

10 mM pan-caspase inhibitor Z-VAD-FMK (Cat# HY-16658B, MCE), or 2 mM JNK inhibitor D-JNKI-1 (JNKi) (Cat# HY-P0069, MCE), or 250 nM DLK inhibitor GNE-3511 (DLKi) (Cat# HY-12947, MCE) was added to the cultured media at day 5 post-AAV infection. 100 nM colchicine (Cat# HY-16569, MCE) or 2 mM etoposide (HY-13629, MCE) was added singly or together to the cultured media at day 7 post-AAV infection or day 14 post-culture. Equal volume of DMSO was added in vehicle control samples. The cell density and LDH analysis was performed after 24–96 hours treatment. The dose of the compounds was chosen to minimize cytotoxicity to the cultured neurons, based on the pilot experiments.

### Immunofluorescent Staining

The cultured neurons on the coverslips were fixed with 4% paraformaldehyde (Santa Cruz, cat# sc-281692) for 20 minutes at 4 °C. After washing with 1x PBS for 3 times, the cells were incubated in 0.2% Triton X-100 for 20 minutes. After rinsing the cells with PBS twice and pre-incubating them with a blocking buffer of 10% normal donkey serum (Cat# S30-100ML, Millipore) and 0.5% Triton X-100 in PBS for 1 h, the cells were incubated with primary antibodies anti-HT7 (Cat# MN1000, Invitrogen, 1:200), Total tau (Cat# T6402, Sigma, 1:300), PHF1 (provided by Dr. Peter Davies, 1:100), AT8 (Cat# MN1020, Invitrogen, 1:200), CP13 (provided by Dr. Peter Davies, 1:100), AT180 (Cat# MN1040, Invitrogen, 1:200), Tau pS262 (Cat# 44-750G, Invitrogen, 1:100), MC1 (provided by Dr. Peter Davies, 1:100), Phospho-Neurofilament H (pNF-H) (Cat# 801601, Biolegend, 1:500), β-Tubulin III (Cat# 801201, Biolegend, 1:500), Synaptophysin (Cat# AF5555, R&D, 1:200), PSD-95 (Cat# 51-6900, Invitrogen, 1:200), HP1α (Cat# 2616, Cell Signaling Technology, 1:200), Phospho-Histone H2A.X (pH2AX) (Cat# 9718, Santa Cruz, 1:100), Lamin A/C (Cat# sc-376248, Santa Cruz, 1:100), Phospho-p53(Ser15) (Cat# 9284, Cell Signaling Technology, 1:200), Active Caspase 3 (Cat# 9664, Cell Signaling Technology, 1:100), Puma (Cat# A3752, Abclonal, 1:500), NeuN (Cat# ABN91, Millipore, 1:500), c-Jun (Cat# A2046, Abclonal, 1:500), Phospho-JNK (p-JNK) (Cat# 4668, Cell Signaling Technology, 1:200), Phospho-c-Jun (p-c-Jun) (Ser73) (Cat# 3270, Cell Signaling Technology, 1:200), p-c-Jun (Ser63) (Cat# AP0105, Abclonal, 1:200), at 4 °C overnight. After 3 separate 10 minutes washes with PBS, they were then incubated with fluorescent secondary antibodies diluted in blocking buffer for 1 hour at room temperature. Following 3 additional PBS washes for 10 minutes each, the cells were counterstained with DAPI, mounted with mounting medium (Cat# P36980, Invitrogen), and photographed using the confocal laser scanning microscopy (Leica, Germany) or EVOS fluorescence microscopy (Life Technologies, USA).

### Immunoblotting

Total protein from cultured neurons were extracted with a cold RIPA lysis buffer composed of protease and phosphatase inhibitor mixtures. The protein concentration was quantified using the BCA assay. The tissue or cell lysate with equal amounts of proteins were subjected to electrophoresis on 8 to 15% SDS-PAGE and then electrophoretically transferred to a PVDF membrane (Bio-Rad tank transfer system, 90V, 90 minutes; Bio-Rad trans-blot turbo system, 25V, 10 minutes). After blocking in 5% milk for 1 h, the membranes were incubated with primary antibodies Total tau (1:2000), HT7 (1:1000), AT8 (1:1000), CP13 (1:1000), AT180 (1:1000), PHF1 (1:1000), p-c-Jun (Ser73, 1:1000), Synaptophysin (1:1000), PSD-95 (1:1000), p-JNK (1:1000), pH2AX (1:500), Active Caspase 3 (1:1000), γ-tubulin (Cat# T6557, Sigma, 1:2000), or β-actin (Cat# sc-47778, Santa Cruz, 1:1000) overnight

at 4 °C. The primary antibody was diluted with 5% BSA in Tris-buffered saline containing 0.05% Tween 20 (TBST) buffer. After three washes with TBST for 10 minutes each, the membranes were incubated with fluor-conjugated Donkey anti-Mouse IgG (Cat# 926-68072, LI-COR, 1:10000), Donkey anti-Rabbit IgG (Cat# 926-68073, LI-COR, 1:10000), or Donkey anti-Goat IgG (Cat# 926-68074, LI-COR, 1:10000) for 1 h. After three times of washing, the signals were visualized by on a LI-COR Odyssey blot imager or Bio-Rad ChemiDoc™ Imagers. The band intensities were normalized to the corresponding value of  $\gamma$ -tubulin or  $\beta$ -actin expression as a loading control. For tau oligomers detection, the method from Dr. Kaye's lab was followed [27] and a pre-cast NuPAGE 4–12% Bis-Tris Gels for SDS-PAGE (NP0335BOX, Invitrogen) was used for oligomeric tau detection.

### Quantitative Real-Time RT-PCR Analysis

Total RNA was preserved in TRIzol solution and extracted with Direct-zol RNA Microprep Kits (Cat# R2062, ZYMO Research). About 200ng–1 $\mu$ g of RNA was used to generate cDNA by reverse transcription using iScript Reverse Transcription Supermix reagent (Cat# 170-8840, Bio-Rad). qRT-PCR was performed using iTaq Universal SYBR Green Supermix (Cat# 172-5124, Bio-Rad) on a CFX384 Touch Real-Time PCR Detection System. The primers used to amplify specific gene products are listed in Table S1. The results of relative quantitative PCR were analyzed using the comparative threshold cycle (Ct) method and normalized to *Hprt1* expression as an endogenous reference.

### RNA-Seq

Total RNA was extracted with Direct-zol RNA Microprep Kits. Novogene Co. (CA, USA) performed mRNA sequencing and data analysis. Basically, the RNA quality was evaluated as follows: RNA integrity number > 7.0 and 28S:18S ratio > 1.8. Messenger RNA was purified from total RNA using poly-T oligo-attached magnetic beads for library construction. The library cDNA was subjected to paired-end sequencing with a pair end 125-base pair reading length on an Illumina HiSeq 2500 sequencer (Illumina, San Diego, CA, USA). For quantification of gene expression level, featureCounts v1.5.0-p3 was used to calculate the reads numbers mapped to each gene. And then FPKM of each gene was determined based on the length of the gene and reads count mapped to this gene. Differential expression analysis was performed using the DESeq2 R package (1.20.0). The P-values were adjusted using the Benjamini and Hochberg's approach for controlling the false discovery rate. Genes with an adjusted P-value  $\leq$  0.05 found by DESeq2 were considered as differentially expressed. ClusterProfiler R package was used to test the statistical enrichment of differential expression genes in KEGG pathways. The local version of analysis tool (<http://www.broadinstitute.org/gsea/index.jsp>), GO, KEGG, Reactome, DO and DisGeNET data sets were used for Gene Set Enrichment Analysis (GSEA).

### Quantification of Axon Degeneration and Neurofilament Fragments in Vitro

The cultured neurons were immuno-stained with  $\beta$ -tubulin III antibody to visualize the microtubule structure, or with Phospho-Neurofilament H (pNF-H) to visualize the neurofilament. For per image, the total number of spheroids on the microtubule and neurofilament fragments was counted by ImageJ software. Then the number was normalized by dividing to the area (pixels) of  $\beta$ -tubulin III or pNF-H positive expression. More than 6 independent areas from 3 individual slides were analyzed for each experimental condition.

### Thioflavin S Staining

Fresh Thioflavin S (ThioS) solution was prepared by dissolving 1 g of ThioS (Cat# T1892, Sigma) in 100ml 80% ethanol, and stirring overnight at 4 °C, and filtering for final use. The fixed cells were rinsed in PBS, then transferred to solution containing 0.0002% thioflavin S in PBS for 8 minutes, rinsed in 40% ethanol in PBS twice for 2 minutes, followed by two rinses in PBS, then mounted on slides.

### Quantification and Statistical Analysis

Statistical analysis was performed using GraphPad Prism 9 (GraphPad Software, San Diego, CA, USA). All data in bar plots are presented as mean  $\pm$  SEM. Data are representative of two or three independent experiments. Unless otherwise noted, differences between two groups were analyzed by two-tailed Student's t-tests, and differences between three or more groups were analyzed by one-way ANOVA with Tukey's multiple comparisons test, as indicated in figure legends. The rate of nuclear envelop invagination between groups was compared by Fisher's exact test.  $p < 0.05$  was considered statistically significant (noted as \* $P < 0.05$ , \*\* $P < 0.01$ , \*\*\* $P < 0.001$  in plots), and those over 0.05 were considered non-significant ("ns", or numerical P values listed in certain plots). All n values are listed in figure legends for each respective plot. All micrographs shown are images representative of multiple replicates as indicated.

## Result

### Neuronal Wild-Type Human Tau Overexpression Prompts Axonal and Neuronal Degeneration

To enable human tau expression, primary mouse neurons were infected at DIV5 with an AAV vector containing the human WT *MAPT* gene (2N4R) under the control of the human *SYN1* promoter (Fig. 1A). Full-length human tau (hTau) protein was produced in the neurons in a time-dependent manner and reached an estimated ratio of 2:1 relative to endogenous mouse

tau protein (Fig. S1A-B). Neuronal hTau expression was further confirmed by immunostaining with a hTau-specific antibody (clone HT7) and a polyclonal antibody that recognizes total

tau protein (both human and mouse) (Fig. 1B). In addition, we detected hTau phosphorylation at multiple amino acid positions (Ser396/Ser404 (PHF-1<sup>+</sup>), Thr231 (AT180<sup>+</sup>), Ser202/Thr205

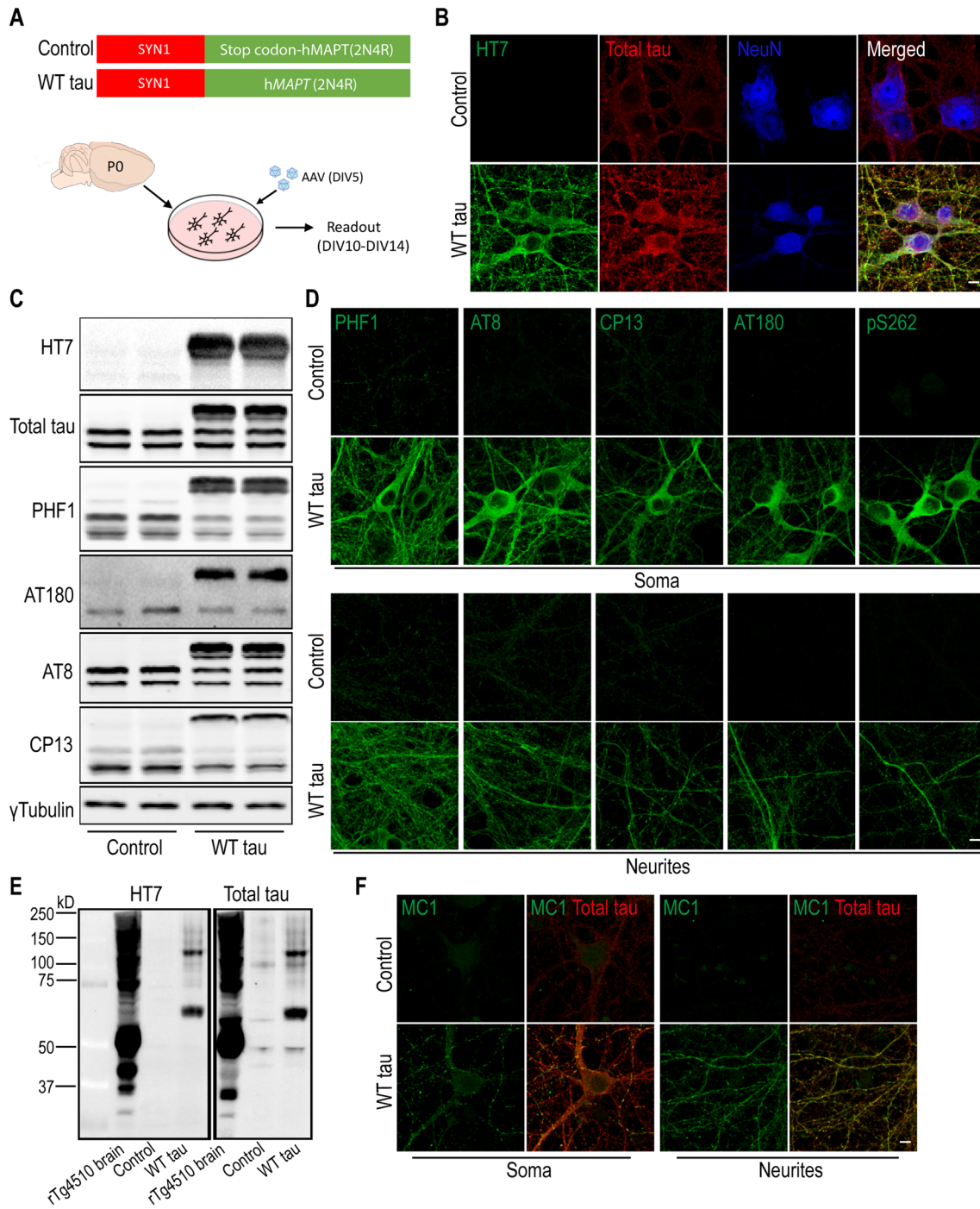


**Fig. 1** Expression of human wild-type tau protein in mouse primary neurons. **(A)** Mouse cortical neurons were cultured *in vitro*. At DIV5, cells were infected either with an AAV vector containing full-length human *MAPT* sequence (2N4R), or a control vector with an inserted stop codon at the N-terminus of the *MAPT* sequence. **(B)** Immunofluorescent staining of tau in neurons (NeuN positive) at day 7 post-infection. The scale bar represents 5  $\mu$ m. **(C)** Western blot results of

tau protein expression in control and WT tau groups. **(D)** Phosphorylated tau visualized in somas and neurites of neurons. The scale bar represents 5  $\mu$ m. **(E)** Tau oligomerization assessed by western blot. Brain lysate of rTg4510 tauopathy mice was used as positive control. **(F)** Presence of misfolded and aggregated tau visualized with antibody MC1. The scale bar represents 5  $\mu$ m.

(AT8<sup>+</sup>), and Ser202 (CP13<sup>+</sup>) (Fig. 1C), which were localized in the soma as well as neurites of the *MAPT*-transduced neurons (Fig. 1D). Hyperphosphorylation can promote tau aggregation and NFT formation [4, 5]. We detected high molecular weight multimeric species of hTau protein by western blot (Fig. 1E) and upregulation of a conformational epitope of aggregated hTau (Fig. 1F); however, no signal was obtained by Thioflavin S staining (Fig. S1C). These findings suggest that WT full-length *MAPT* overexpression in primary neurons leads to human tau hyperphosphorylation and aggregation in the absence of NFT.

Several days after AAV infection, WT hTau<sup>+</sup> neurons started to display morphological changes indicative of degeneration. By day 7 post-infection, we observed gross axonal degeneration manifested by the development of numerous axon swelling or spheroids (Fig. 2A) and the accumulation of fragmented neurofilaments in culture (Fig. 2B). In conjunction, synaptic markers were significantly reduced

(Figs. 2C and D). By day 9 post-infection, neuronal density was decreased by > 80% in WT hTau<sup>+</sup> culture (Fig. 2E). Moreover, by assaying the culture medium longitudinally, we detected a time-dependent escalation of lactate dehydrogenase (LDH) release, corroborating a remarkable neurotoxic phenotype of intracellular WT human tau in primary neurons (Fig. 2F).

### Caspase 3 Activation is Involved in WT hTau-Dependent Neurodegeneration

To investigate the neurotoxicity elicited by WT hTau, we first examined apoptosis, a programmed cell death pathway that has been implicated in the loss of neurons in AD [28]. Apoptotic death involves the function of caspases, among which caspase 3 activation serves as a central effector [29]. In WT hTau<sup>+</sup> neurons, we detected increased abundance of cleaved caspase 3, the signal

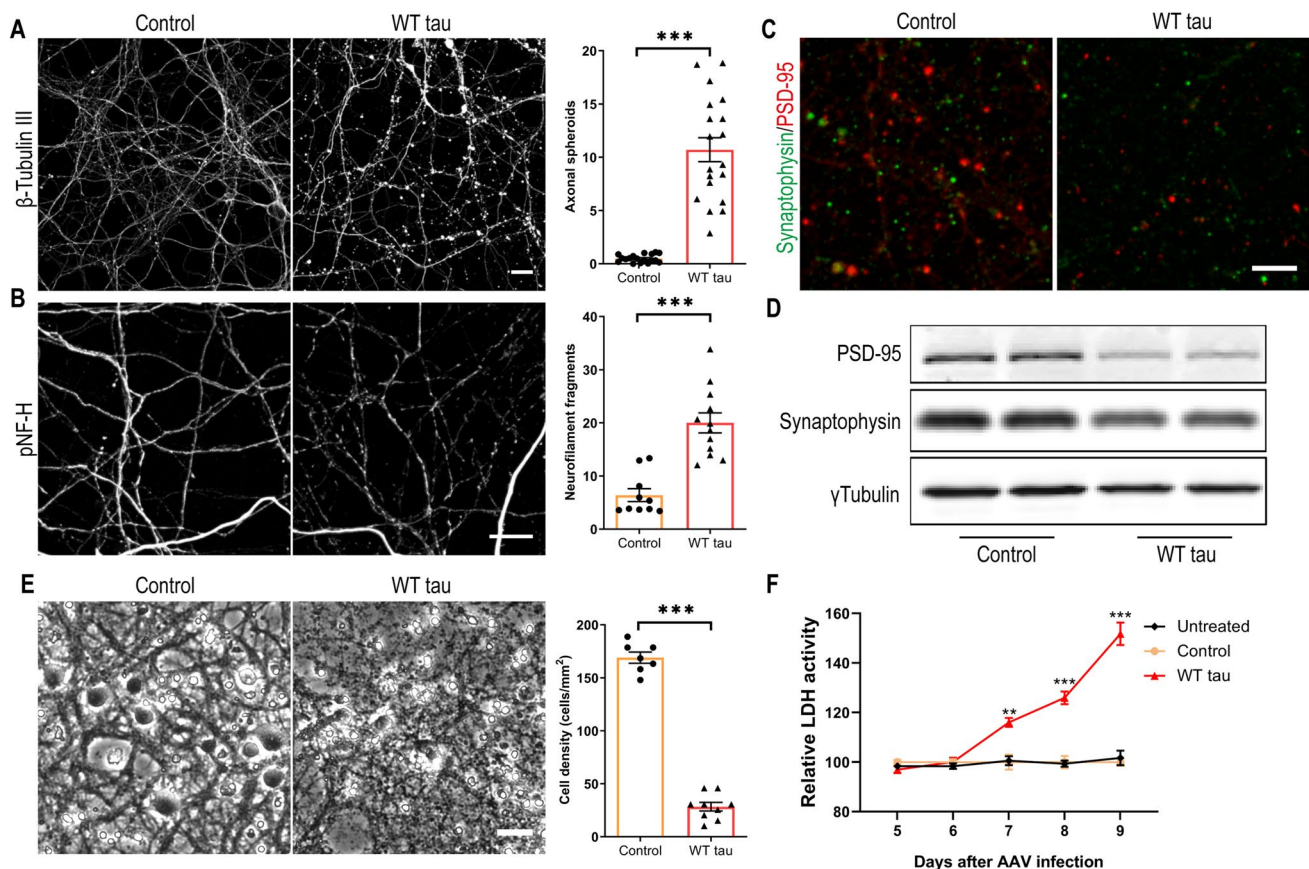


**Fig. 2** Axonal degeneration and cell death in WT hTau-expressing neurons. **(A)** Representative images of  $\beta$ -tubulin III staining in control and WT tau groups at day 7 post-infection and quantification of axonal spheroids. The scale bar represents 10  $\mu$ m. n=18, 19 individual images in control, WT tau groups, respectively. **(B)** Representative images of phosphorylated neurofilament heavy chain (pNF-H) staining in control and WT tau groups at day 7 post-infection and quantification of neurofilament fragments. The scale bar represents 10  $\mu$ m. n=10, 12 individual images in control, WT tau groups, respec-

tively. **(C)** Representative images of PSD-95 and synaptophysin co-staining in control and WT tau groups. The scale bar represents 5  $\mu$ m. **(D)** Western blot results of PSD-95 and synaptophysin expression in control and WT tau groups. **(E)** Representative cell images in control and WT tau groups at day 9 post-infection and quantification of cell density. The scale bar represents 25  $\mu$ m. n=7, 9 individual images in control, WT tau groups, respectively. **(F)** Kinetic analysis of LDH activity in the culture media from untreated, control and WT tau groups. n=6 wells/group in each time point.

of which was present both inside the nuclei and in the neuritic areas rich with axonal spheroids (Figs. 3A and B). Consistently, WT hTau<sup>+</sup> neurons expressed more *Casp3* mRNA (Fig. 3C). PUMA, encoded by the *Bbc3* gene, is critically involved in the intrinsic apoptotic signaling pathway [30]. We detected elevated

expression of both mRNA and protein products of *Bbc3* in neurons with WT hTau (Figs. 3D and E). To test the importance of caspase activity in tau-induced degeneration, we treated WT hTau<sup>+</sup> neurons with pan-caspase inhibitor Z-VAD-FMK and observed a significant lessening of neurotoxicity (Figs. 3G and

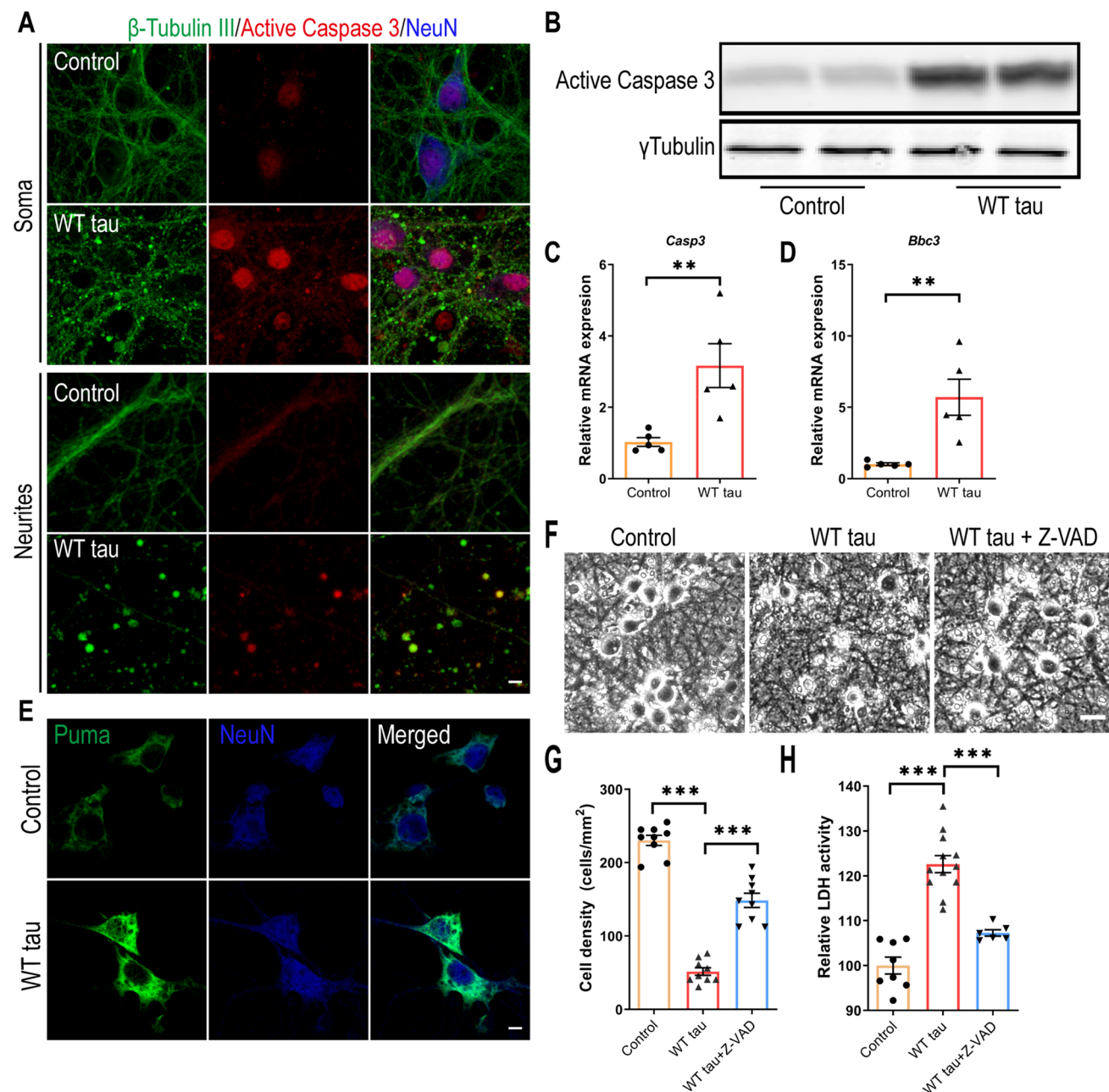
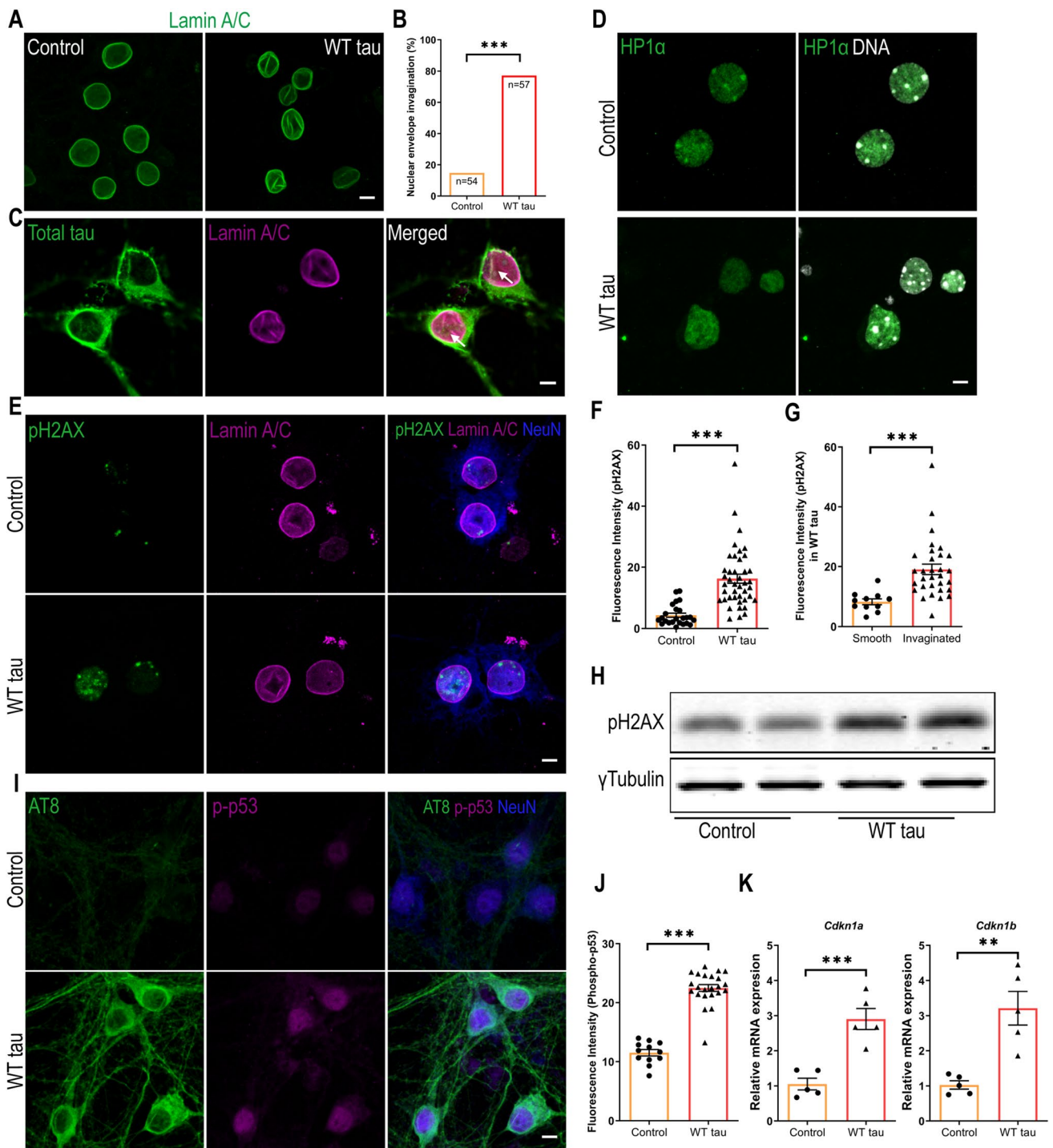


**Fig. 3** Caspase 3 activation in WT hTau-expressing neurons. **(A)** Representative images of  $\beta$ -tubulin III and active caspase 3 co-staining in somas and neurites at day 7 post-infection. The scale bar represents 5  $\mu$ m. **(B)** Active caspase 3 expression assessed by western blot. **(C)** Relative expression of *Casp3* mRNA at day 7 post-infection. n=5 samples/group. **(D)** Relative expression of *Bbc3* mRNA at day 7 post-infection. n=5 samples/group. **(E)** Representative images of Puma staining in control and WT Tau-expressing neurons. The scale bar represents 5  $\mu$ m. **(F)** Representative cell images in control or WT

tau groups with or without pan-caspase inhibitor Z-VAD-FMK treatment. The scale bar represents 25  $\mu$ m. **(G)** Quantification of cell density 72 hrs after the treatment as shown in **F**. n=9 individual images/group. **(H)** Relative LDH activity 72 hrs after the treatment as shown in **F**. n=8, 12, 6 wells in control, WT tau, WT tau + Z-VAD groups, respectively. Data are presented as mean  $\pm$  SEM. Statistical significance was determined using unpaired, two-tailed Student's t test in C and D, or one-way ANOVA with Tukey's multiple comparisons test in G and H.



H). These results suggest that caspase 3 activity contributes to WT human tau-driven neurodegeneration.

### Wild-Type hTau Induces DNA Damage Response in Neurons

To probe the mechanistic connection between tau and apoptosis, we assessed the nuclei of neurons expressing WT hTau. Lamins are architectural proteins that confer

mechanical stability to the nuclear envelope [31]. Visualization of nuclear lamins revealed that, in the presence of WT hTau, many neurons displayed abnormal invaginations in their nuclear membrane (Figs. 4A and B). Further analysis revealed the colocalization of hTau with ruffled lamin A/C signals in the nuclear envelope (Fig. 4C), suggesting a physical presence of WT hTau at sites of disruption.

Nuclear envelope disturbance can have serious consequences for a cell, particularly detrimental for chromatin and



**Fig. 4** DNA damage response in WT hTau-expressing neurons. (A) Representative images of lamin A/C staining in control and WT tau groups at day 7 post-infection. The scale bar represents 5  $\mu$ m. (B) Quantification of nuclear envelope invagination rate in control and WT tau groups.  $n=54, 57$  neurons in control and WT tau groups, respectively. (C) Representative images of total tau and lamin A/C co-staining in WT tau group. The white arrows indicate colocalization of tau and lamin A/C in the invaginated area of nuclear membrane. The scale bar represents 5  $\mu$ m. (D) Representative images of HP1 $\alpha$  staining (green) in control and WT tau groups. Genomic DNA stained by DAPI is shown in white. The scale bar represents 5  $\mu$ m. (E) Representative images of pH2AX and lamin A/C co-staining in control and WT tau groups at day 7 post-infection. The scale bar represents 5  $\mu$ m. (F) Quantification of nuclear pH2AX signals from cultures shown in E.  $n=24, 42$  neurons in control and WT tau groups, respectively. (G) Quantification of nuclear pH2AX signals in WT tau-expressing neurons with smooth or invaginated membrane.  $n=11$  neurons with smooth nuclear membrane;  $n=31$  neurons with invaginated membrane. (H) Western blot result of pH2AX expression in control and WT tau groups. (I) Representative images of AT8 and phospho-p53 (p-p53) co-staining in control and WT tau groups at day 7 post-infection. The scale bar represents 5  $\mu$ m. (J) Quantification of nuclear p-p53 signals from cultures shown in I.  $n=12, 23$  neurons in control and WT tau groups, respectively. (K) Quantitative RT-PCR result of relative *Cdkn1a* and *Cdkn1b* mRNA expression in control and WT tau groups at day 7 post-infection.  $n=5$  samples/group. Data are presented as mean  $\pm$  SEM. Statistical significance was determined using the Fisher's exact test in B, or unpaired, two-tailed Student's t-test in F, G, J and K.

genomic stability [31]. We found that WT hTau<sup>+</sup> neurons displayed fewer nuclear foci of heterochromatin protein 1 $\alpha$  (HP1 $\alpha$ ), an indication of the loss of chromatin compactness (Fig. 4D). Phosphorylated Ser-139 of the histone variant H2AX (pH2AX) is a sensitive molecular marker of double-strand DNA (dsDNA) damage and repair [32]. Inside the nuclei of WT hTau<sup>+</sup> neurons, we detected significantly increased pH2AX signal intensity, which correlated with the higher abundance of pH2AX protein in the cells (Figs. 4E, F and H). Furthermore, we found heightened nuclear pH2AX signal in cells exhibiting nuclear membrane invagination (Fig. 4G), suggesting a functional connection between nuclear envelope disruption and DNA damage response (DDR).

Activation of the well-known tumor suppressor p53 occurs in response to DNA damage and other cellular stresses and plays a critical role in apoptosis [33]. In conjunction with the pH2AX signal, phospho-p53 protein was detected in the nuclei of WT hTau<sup>+</sup> neurons (Fig. 4I, J). During DDR, p53 induces cell cycle regulatory proteins to elicit intrinsic checkpoint control [34]. Accordingly, we found that WT hTau<sup>+</sup> neurons increased the transcription of *Cdkn1a* and *Cdkn1b*, which encode inhibitors for cyclin-dependent kinases (Fig. 4K). These results collectively pinpoint a prevalent DNA damage response that is triggered by WT human tau in differentiated neurons.

## DLK-MAPK Signaling Partakes in WT hTau-Dependent Neurodegeneration

To gain deeper molecular insights into the cellular pathways that are affected by WT hTau, we performed RNAseq analysis on the AAV-transduced neurons. A significant number of genes were differentially regulated between the AAV control and WT hTau<sup>+</sup> neurons. Among these, multiple apoptosis and cell death-related genes displayed significantly higher levels of expression in WT hTau<sup>+</sup> neurons (Fig. S2A). KEGG pathway analysis further revealed multiple significantly affected cellular processes (Fig. 5A; supplemental data S1). Consistent with the observed axonal and synaptic degeneration, “axon guidance” and “synaptic vesicle cycle” represented the topmost significantly altered processes. Interestingly, the “MAPK signaling pathway” contained the greatest number of genes significantly affected by WT hTau (Fig. 5A). Among the genes differentially upregulated by WT hTau, *Jun* proto-oncogene ranked highest by the adjusted *p* value (Fig. 5B; supplemental data S2).

c-Jun, the protein product of *Jun*, can be phosphorylated by c-Jun N-terminal kinases (JNKs), a subset of MAP kinases, and subsequently translocate to nucleus to take a part in the transcriptional activity of AP-1 [35]. Consistent with the upregulation of the *Jun* transcript, the c-Jun protein was expressed more abundantly and exhibited a nuclear enrichment in WT hTau<sup>+</sup> neurons (Fig. 5C). Moreover, phosphorylated c-Jun at both serine 63 and serine 73 increased in these cells, which was exclusively present inside the nuclei (Figs. 5D, F, G, and S2B-C). In addition, we detected highly elevated nuclear phospho-JNK expression in many WT hTau<sup>+</sup> neurons (Figs. 5D, E, G). Together with the RNA profiling results, these findings uncover a substantially activated MAPK-JNK pathway in degenerating WT hTau<sup>+</sup> neurons. JNK has both pro- and anti-apoptotic functions, depending on many complex factors [36]. To gauge its involvement in our model, we deployed a selective JNK inhibitor at a dose effective to diminish the activities of JNK and c-Jun in the culture of WT tau<sup>+</sup> neurons (Figs. 5D-F) and observed substantial reduction of neurotoxicity with the treatment (Figs. 5H-J).

DLK is a MAP3K functionally involved in axonal degeneration as well as regeneration, generally in sync with the activities of JNKs and c-Jun [37–40]. We hypothesized that DLK activity may serve as a key node of the MAPK pathway in WT hTau<sup>+</sup> neurons thus decided to examine the potency of an established DLK inhibitor to curb JNK/c-Jun signaling [41]. Similar to the JNK inhibitor, DLK inhibition effectively repressed the activities of JNK and c-Jun in hTau<sup>+</sup> neurons (Figs. 5D-F). More potent than the JNK inhibitor, DLK inhibition significantly rescued the neurons from WT hTau-induced neurotoxicity (Fig. 5H-J). Altogether, we have

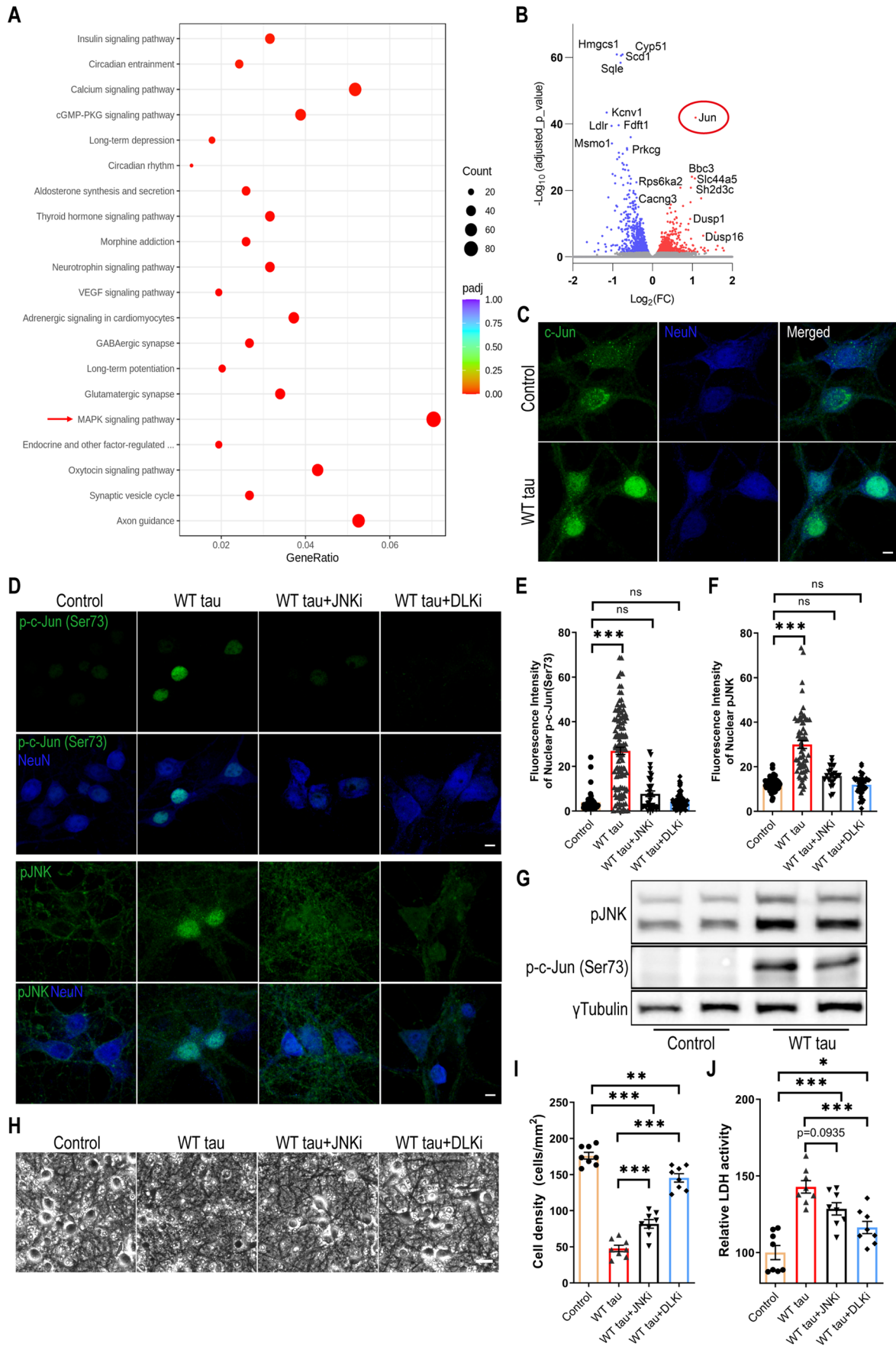


**Fig. 5** MAPK-DLK signaling in WT hTau-expressing neurons. **(A)** Top 20 most significantly affected KEGG pathways in WT tau group, compared with control group. **(B)** Volcano plot showing the top most differentially expressed genes (DEG) by WT tau. **(C)** Representative images of c-Jun staining in control and WT tau groups. The scale bar represents 5  $\mu\text{m}$ . **(D)** Representative images of p-c-Jun (Ser73) and pJNK staining in control or WT tau grouped with or without JNK inhibitor (JNKi) or DLK inhibitor (DLKi) treatment. The scale bar represents 5  $\mu\text{m}$ . **(E)** Quantification of nuclear pJNK signals from cultures shown in **D**.  $n=45, 115, 34, 90$  neurons in control, WT tau, WT tau + JNKi, WT tau + DLKi groups, respectively. **(F)** Quantification of nuclear p-c-Jun (Ser73) signals from cultures shown in **D**.  $n=59, 62, 23, 37$  neurons in control, WT tau, WT tau + JNKi, WT tau + DLKi groups, respectively. **(G)** Western blot result of pJNK and p-c-Jun (Ser73) expression in control and WT tau groups. **(H)** Representative cell images in control or WT tau groups with or without JNKi or DLKi treatment. The scale bar represents 25  $\mu\text{m}$ . **(I)** Quantification of cell density from cultures shown in **H**.  $n=8$  images/group. **(J)** Quantification of relative LDH activity in culture media of cells shown in **H**.  $n=8$  wells/group. Data are presented as mean  $\pm$  SEM. Statistical significance was determined using one-way ANOVA with Tukey's multiple comparisons test in E, F, I and J.

identified MAPK-DLK signaling as a significant contributor to WT hTau-induced neurodegeneration.

### P301L hTau Overexpression Differentially Affects Primary Neurons

The P301L missense mutation in *MAPT* is causally associated with human FTLN and has been extensively studied in various tauopathy models [14, 15]. To compare its functional impact relative to WT hTau, we similarly infected primary neurons with P301L *MAPT* packaged into an identical AAV vector to achieve equivalent overexpression. By morphological examination and measurement of LDH release, we unexpectedly observed a reduced extent of neurodegeneration by P301L hTau in side-by-side examination with WT hTau (Figs. 6A–C). Consistently and significantly, P301L hTau induced less cytotoxicity than WT hTau on primary neurons in all time points examined (Fig. S3A). In line with these observations, we detected lower amounts of activated caspase 3 protein in mutant hTau<sup>+</sup> neurons (Figs. 6D and E). To comprehend the underlying mechanism, we carefully compared the hTau protein expression and found that P301L hTau was somewhat less phosphorylated, even though the total abundance of transgenic tau protein was slightly higher than in cells expressing WT hTau (Figs. 6D–F, S1A). Despite a ubiquitous distribution of the mutant hTau protein, phosphorylated P301L hTau was largely restricted to somas of neurons, an intriguing contrast to phosphorylated WT hTau which abundantly associated with axons and dendrites (Fig. 6F). No thioflavin S<sup>+</sup> signal was detected in these cells (Fig. S3B), suggesting the lack of NFT deposition, similar to WT hTau.

For a deeper understanding of changes initiated by mutated tau, we profiled the transcriptome of P301L hTau<sup>+</sup>

neurons and obtained a list of genes that were differentially regulated by the mutant tau. Pathway analysis revealed that P301L hTau significantly affected processes such as “electron transport chain”, “mitochondrial protein complex”, and “ribosome/ribosomal subunit” (Fig. 6H; supplemental data S3). By contrast, WT hTau altered the expression of over 1600 genes in neurons, more than 3 times over mutant hTau (Fig. 6G; supplemental data S2). A direct genome-wide comparison between WT and P301L hTau<sup>+</sup> neurons uncovered selective alterations of “axon guidance” and “apoptosis” by WT hTau, and “ribosome” and “oxidative phosphorylation” by P301L hTau (Fig. S3C). In terms of DNA damage response, the two hTau forms elicited similar gene expression profiles (Fig. 6I); however, P301L hTau did not disrupt MAPK pathway genes as did the WT hTau (Fig. 6I).

To confirm these findings, we examined P301L hTau<sup>+</sup> neurons and detected many cells with invaginated nuclear envelope, similar to WT hTau<sup>+</sup> neurons (Figs. 6J and K). Likewise, increased pH2AX signal, comparable with WT hTau, was detected in P301L hTau<sup>+</sup> neurons (Figs. 6L–N). By contrast, P301L hTau<sup>+</sup> neurons contained much lower detectable levels of phospho-c-Jun in their nuclei in comparison with WT hTau (Figs. 6M and O), consistent with RNAseq profiling showing a major difference in MAPK pathway between the two forms of hTau. Moreover, P301L hTau<sup>+</sup> neurons showed little sign of axonal degeneration (Fig. S3D). Altogether, our investigation reveals that P301L hTau overexpression differentially affected primary neurons other than WT hTau in many important aspects.

### DNA Damage Response and DLK-MAPK Signaling Synergistically Promote Neurodegeneration

To comprehend the relationship between DDR and MAPK-DLK activation in WT tauopathy, we took a closer look at the WT hTau<sup>+</sup> neurons by dual immunostaining of pH2AX and phospho-c-Jun and detected more cells expressing the marker of DDR than those with MAPK signaling (Fig. 7A). We did not find a significant correlation between the levels of the two markers on a per cell basis, but noticed a general lack of cells solely expressing nuclear phospho-c-Jun (Figs. 7A and B). Interestingly, WT hTau<sup>+</sup> neurons treated with DLK inhibitor did not diminish the pH2AX signal (Figs. 7C and D), suggesting that DNA damage response is either upstream or independent of MAPK-DLK signaling.

Pathogenic tau is known to modify cytoskeletal functions by dissociating from microtubules and intercepting F-actin [42, 43]. Having observed distinct distribution patterns of WT and P301L phospho-hTau (Fig. 6F) and selective accumulation of activated caspase 3 in axonal spheroids in WT hTau<sup>+</sup> neurons (Fig. 2A), we hypothesized that 1) axonal WT hTau may stimulate MAPK-DLK signaling by

inducing axonal degeneration independently from somatic hTau-induced DDR; and 2) MAPK-DLK signaling and DDR function synergistically in WT hTau<sup>+</sup> neurons, whereas lack of axonal DLK activation renders P301L tau less neurotoxic. To test this hypothesis, we adopted a selective inhibitor of microtubule formation [44], as disruption of microtubule dynamics is known to cause DLK-mediated axonal swelling and degeneration [45]. Low-dose colchicine treatment robustly induced nuclear phospho-c-Jun accumulation without any sign of DDR in primary neurons (Figs. 7E and F). We also used etoposide, a chemotherapy agent capable of inducing dsDNA breaks: primary neurons exposed to low-dose etoposide readily upregulated nuclear pH2AX expression (Fig. S4). Individually, these compounds caused limited toxicity in neurons after 48 hours; however, combined treatment resulted in severe cell loss and LDH release, indicating a powerful synergistic effect of axonal stress and DDR in neurodegeneration (Figs. 7G–I). To further demonstrate the interaction between these pathways in the tau-relevant situation, we treated P301L hTau<sup>+</sup> neurons with low-dose colchicine and observed significantly expedited degeneration in culture (Figs. 7J–L). In summary, these findings uncover a striking synergistic interplay between DNA damage response and the MAPK-DLK axis in AD-relevant neurodegeneration.

## Discussion

In this study, we investigated the consequence of human tau overexpression in primary neurons and discovered a pathogenic coupling of DNA damage response and DLK-MAPK signaling in wild-type hTau-mediated neurotoxicity. By contrast, P301L hTau, which is associated with FTL, elicited primarily the DNA damage response, with less aggressive neurodegeneration (Fig. 8). The overt WT hTau-induced pathology was highly significant and reproducible, yet somewhat unexpected. Historically, non-mutant *MAPT*-expressing mouse strains either develop no CNS NFT or limited tangle pathology only when the animals are aged [14, 15]. Instead, overexpression of mutant *MAPT* genes results in robust NFT deposition in rodent brains, which led to the wide adaptation of the mutant models to study tauopathy. It becomes clear now that transgene expression *in vivo* is grossly affected by the promoter of choice as well as transgene copy number and insertion sites, making it difficult to directly compare different transgenic lines. Interestingly, Gamache *et al* constructed genetically matched transgenic mice overexpressing WT or P301L 0N4R hTau and observed greater pathogenicity in WT hTau<sup>+</sup> animals, including exaggerated tau hyperphosphorylation and early cognitive impairment [46]. Although we studied the 2N4R

isoform *in vitro*, the phenotypic disparity between WT and mutant hTau is highly analogous.

AD and other tauopathies may affect different brain regions, thus their pathogenesis can be mediated by different types of neurons, circuits, and other cell types under the influence of distinct local signals. Nevertheless, our cortical neuron culture revealed a remarkable contrast between WT and mutant hTau in altering key cellular processes, highlighting a keen influence by the identity of the tau protein itself in disease progression. Extensive biochemical and biophysical characterization has revealed structural distinctions between NFTs formed under different tauopathy conditions, of which sensitive tracers can be applied to detect their deposition by positron emission tomography [47, 48]. In addition to altered binding to microtubules, WT hTau interacts with a long list of cellular proteins not observed with FTL-associated mutants [20, 43, 49, 50]. For example, Tracy *et al* performed an in-depth analysis of the tau interactome in human iPSCs and reported preferential interaction of WT tau with mitochondria and impaired bioenergetics by FTL-tau [20]. Not so surprisingly, WT and mutant hTau also differentially affect the global transcriptome. Using tau-inducible HEK cells, Montalbano *et al* reported that WT hTau affected a higher number of genes than P301L mutant, including those involved in cytoskeleton-dependent processes, while P301L hTau perturbed pathways associated with reactive oxygen species [21]. In fully differentiated neurons, we similarly observed more profound influence of WT hTau on transcriptome (Fig. 6H) and detected selective effects on “axon guidance” and “apoptosis” by WT hTau, and “ribosome” and “oxidative phosphorylation” by P301L hTau (Fig. S3).

AD and tauopathies are associated with numerous nuclear irregularities, which include excessive DNA damage [51, 52], altered DNA repair [27, 53], cell cycle re-entry [25, 54], chromosomal defects [55] and senescence [56, 57]. Long linked to brain aging and neurodegeneration, neuronal DNA damage, manifested by pH2AX<sup>+</sup> foci, accumulates early in AD brain [56, 57]. Here, we detected comparable levels of pH2AX signal associated with WT and mutant hTau in primary neurons. Very low levels of tau localizes inside the nuclei of healthy neurons, where it plays a role in regulating genome stability and nucleolar function [58]. Although we did not observe increased nuclear tau, our characterization revealed close proximity of hTau with the nuclear membrane, which is accompanied by significant nuclear envelope deformation (Figs. 4 and 6). This finding is consistent with earlier reports on human AD as well as the aberrant interaction between pathogenic tau and nuclear pore components [59–63]. Nuclear envelope disruption may also impair the structures that anchor heterochromatin and cause genomic injury [64]. Our examination revealed abnormal heterochromatin relaxation and dsDNA damage response in hTau<sup>+</sup> neurons (Fig. 4). While tau-associated global chromatin

relaxation has been reported in human AD and identified as a toxic effector of neurodegeneration in a tauopathy model, tau accumulation was also shown to trigger DDR by various studies [27, 63, 65, 66]. DNA damage is a well-known stress inducer of apoptosis [67]. In WT hTau<sup>+</sup> neurons, we observed an enrichment of the “apoptosis” pathway, the upregulation of several prototypical executors of apoptosis, such as caspase-3 and PUMA, and detected the functional involvement of caspase activation (Figs. 3, S2 and S3).

Neurons are highly sensitive to stress, which can activate multiple signaling pathways and eventually lead to cell death governed by a variety of mechanisms [68, 69]. Axonal degeneration is of particular importance, as axonal cytoskeleton integrity is essential for many neuronal functions, such as long-range cargo transport and transmission of action potentials [70]. We have detected several hallmarks of axonal degeneration in WT hTau<sup>+</sup> neurons: prominent formation of axonal spheroids colocalized with activated

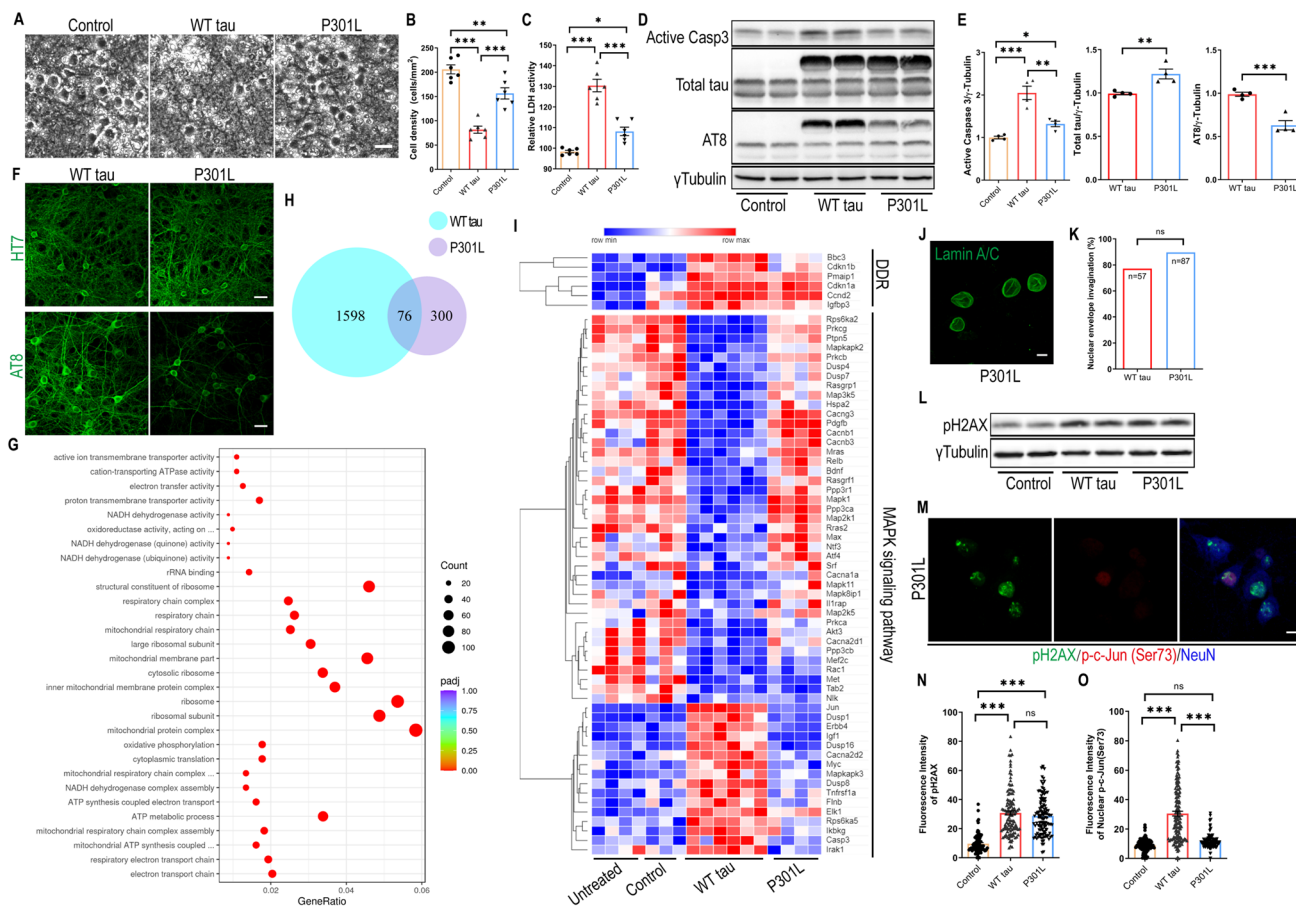


**Fig. 6** Differential effects of P301L and WT hTau on primary neurons. **(A)** Representative cell images in control, WT tau, P301L tau (P301L) groups at day 9 post-infection. Scale bar represents 25  $\mu$ m. **(B)** Quantification of cell density from cultures shown in **A**.  $n=6$  images/group. **(C)** Relative LDH activity in culture media from cultures shown in **A**.  $n=6$  wells/group. **(D)** Western blot showing active caspase 3, total tau and AT8 expression in control, WT tau and P301L tau groups at day 7 post-infection. **(E)** Quantification of active caspase 3, exogenous total tau and AT8 expression.  $n=4$  samples/group. **(F)** Representative images of HT7 and AT8 staining in WT tau or P301L tau groups. The scale bar represents 20  $\mu$ m. **(G)** Top 30 most significantly affected pathways in P301L tau group, compared with control group. **(H)** Venn diagram of DEGs affected by WT versus P301L tau in neurons. **(I)** Heatmap showing differential expression of DNA damage response (DDR) and MAPK signal pathway genes among different groups. The rows in the heatmap were sorted by similarity via hierarchical clustering. **(J)** Representative images

of lamin A/C staining in P301L group. The scale bar represents 5  $\mu$ m. **(K)** Quantification of nuclear envelope invagination rate in WT tau and P301L tau groups.  $n=57, 87$  neurons in control and WT tau groups, respectively. **(L)** Western blot result of pH2AX expression in control, WT tau and P301L tau groups at day 7 post-infection. **(M)** Representative images of pH2AX and p-c-Jun (Ser73) co-staining in P301L tau group. The scale bar represents 5  $\mu$ m. **(N)** Quantification of pH2AX signals in control, WT tau, and P301L tau groups.  $n=82, 124, 123$  neurons in control, WT tau, P301L tau groups, respectively. **(O)** Quantification of nuclear p-c-Jun (Ser73) signals in control, WT tau, P301L tau groups.  $n=130, 146, 120$  neurons in control, WT tau, P301L groups, respectively. Data are presented as mean  $\pm$  SEM. Statistical significance was determined using unpaired, two-tailed Student's  $t$  test in **E** (total tau and AT8), Fisher's exact test in **K**, or one-way ANOVA with Tukey's multiple comparisons test in **B**, **C**, **E** (active caspase 3), **N** and **O**.

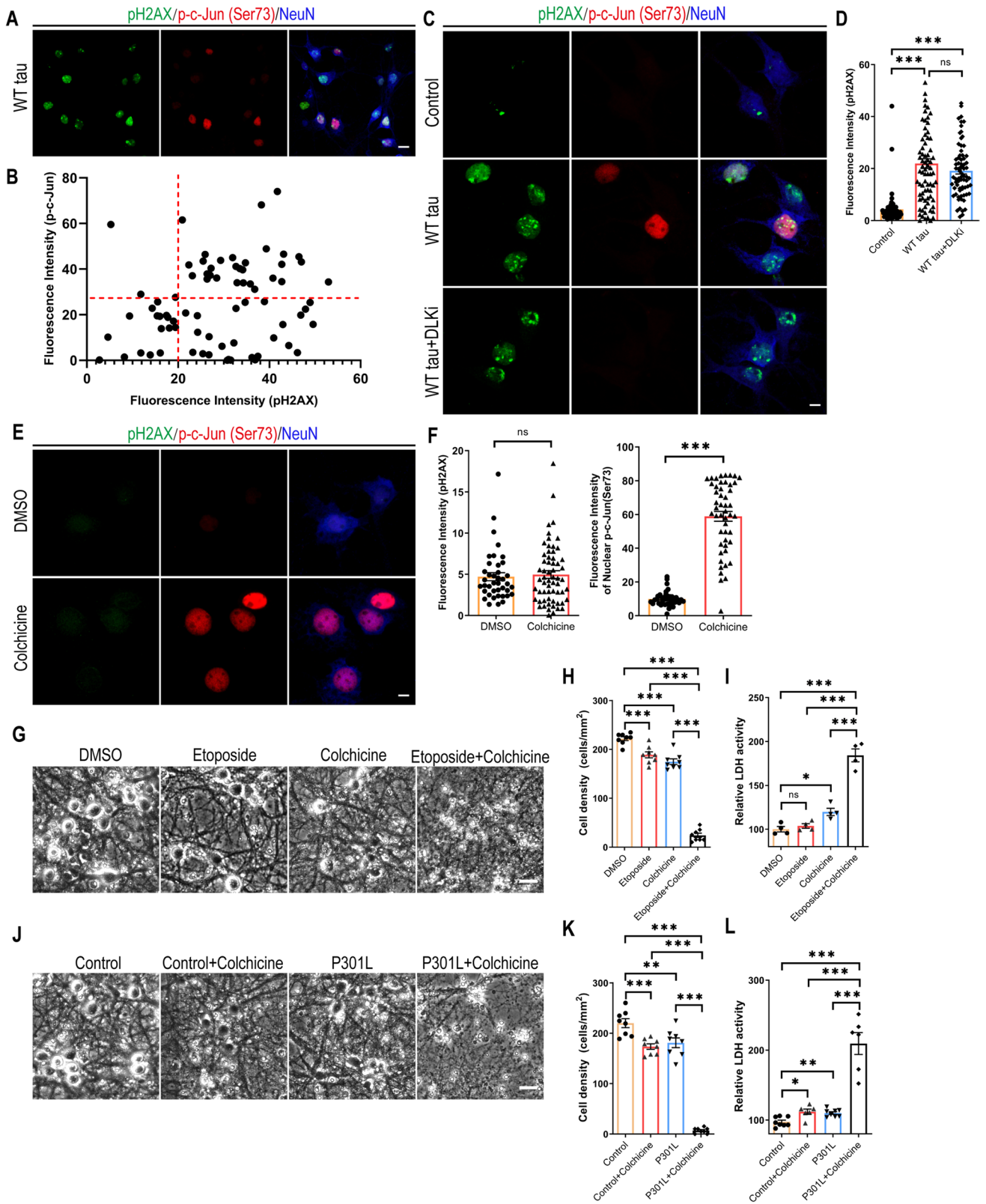


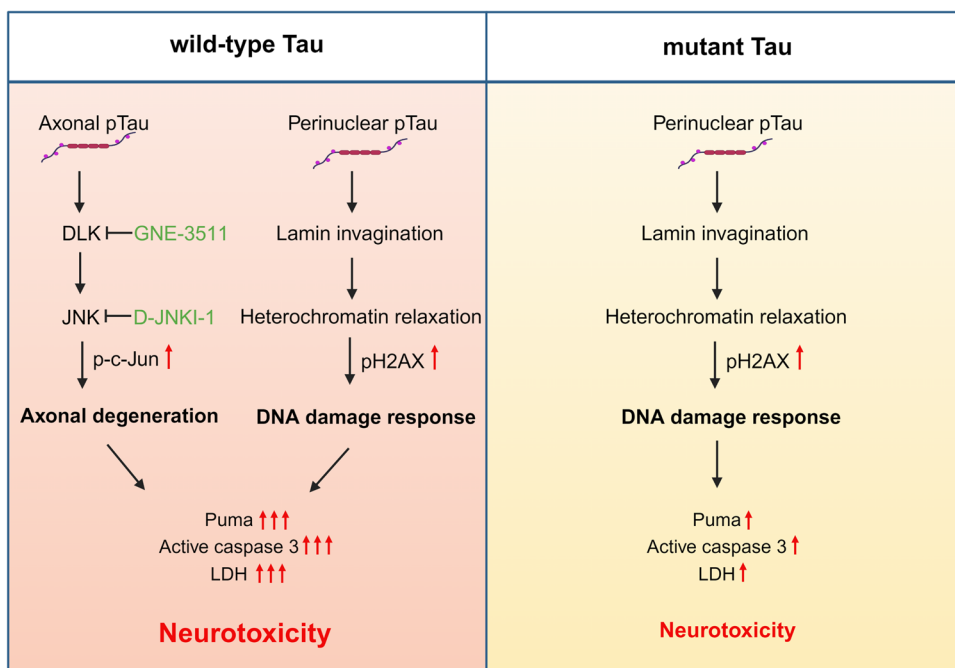
**Fig. 7** Synergy between DNA damage response and MAPK-DLK signaling in neurodegeneration. **(A)** Representative images of pH2AX and p-c-Jun (Ser73) co-staining in WT tau group. The scale bar represents 10  $\mu\text{m}$ . **(B)** The correlation analysis of nuclear pH2AX and p-c-Jun (Ser73) signals in culture as shown in **A**. Total of 76 neurons were subjected to Pearson correlation analysis.  $R^2=0.0492$ ,  $p=0.0542$ . **(C)** Representative images of pH2AX and p-c-Jun (Ser73) co-staining in control and WT tau groups with or without DLK inhibitor treatment. The scale bar represents 5  $\mu\text{m}$ . **(D)** Quantification of nuclear pH2AX signals in cultures as shown in **C**.  $n=63, 78, 72$  neurons in control, WT tau, WT tau + DLKi groups, respectively. **(E)** Representative images of pH2AX and p-c-Jun (Ser73) co-staining in vehicle DMSO- and colchicine-treated groups. The scale bar represents 5  $\mu\text{m}$ . **(F)** Quantification of nuclear pH2AX and p-c-Jun (Ser73) signals in cultures as shown in **C**.  $n=41, 50$  neurons in DMSO, colchicine groups, respectively. **(G)** Representative cell images in groups treated with DMSO, etoposide, colchicine, and etoposide plus colchicine. The scale bar represents 25  $\mu\text{m}$ . **(H)** Quantification of cell density in cultures as shown in **G**.  $n=8$  images/group. **(I)** Relative LDH activity in culture media of cells as shown in **G**.  $n=4$  wells/group. **(J)** Representative cell images in control and P301L tau groups, treated with vehicle or colchicine. The scale bar represents 25  $\mu\text{m}$ . **(K)** Quantification of cell density in cultures as shown in **J**.  $n=8$  images/group. **(L)** Relative LDH activity in culture media of cells as shown in **J**.  $n=8, 6, 8, 6$  wells in the above groups, respectively. Data are presented as mean  $\pm$  SEM. Statistical significance was determined using one-way ANOVA with Tukey's multiple comparisons test in **D, H, I, K** and **L**, or unpaired, two-tailed Student's *t* test in **F**.

caspase 3 and accumulation of fragmented neurofilaments, accompanied by the loss of synapses and eventual release of LDH and cell death (Figs. 2 and 3). In contrast, little axonal degeneration was detectable in P301L hTau<sup>+</sup> neurons (Fig. S3D). Coincidentally, we found that WT hTau, hyperphosphorylated and aggregated, is abundantly distributed

throughout the axons and dendrites. This is in sharp contrast with P301L hTau, which was largely restricted to the soma of neurons when phosphorylated (Figs. 2 and 6). Consistent with our *in vitro* findings, axonopathy represents the most robust pathological feature exhibited by various WT hTau animal models *in vivo*, which was remarkably absent in mutant *MAPT*-expressing brains [71–74].

The activity of DLK, a neuron-specific MAP3K, is centrally involved in both axonal degeneration and regeneration, and its pathogenic role has been implicated in neurodegeneration [41, 75]. Intriguingly, DLK's downstream target JNK and its substrate c-Jun were increased in WT hTau<sup>+</sup> neurons, mirrored by the enrichment of the MAPK pathway in these cells (Fig. 5). Furthermore, we showed that pharmacological inhibition of DLK was highly effective in rescuing WT hTau<sup>+</sup> neurons, implying a prominent role played by the DLK-MAPK axis in AD-relevant neurodegeneration (Fig. 5). Axonopathy and transport deficits occur early in the pathogenesis of AD when axonal swellings are abundant near the amyloid plaques [76]. Not merely appearing in Braak I–III, phospho-tau<sup>+</sup> axonal spheroids continuously and robustly build up in later stages (Braak IV–VI) of the disease [76–78]. Remarkably, expression of phospho-JNK and phospho-c-Jun correlates positively with phosphorylated pathogenic tau in AD brains [41]. Notably, the MAPK pathway has been independently identified by recent proteomic studies as one of the most significantly affected processes in AD [79, 80]. Hence, our findings from a cellular tauopathy model here offer mechanistic insight into how the DLK-JNK-c-Jun axis, one discrete branch of the MAPK cascade, may directly partake in neuron-intrinsic degeneration in AD.

**Fig. 8** Schematic of intraneuronal tau-induced neurodegeneration. Wild-type and mutant human tau exhibit differential toxic effects on primary neurons. Wild-type tau triggers DLK-MAPK-mediated axonal degeneration and DNA damage response, which synergistically promote overt neurotoxicity. Mutant tau primarily produces DNA damage response, with less severe toxic effect.



Sporadic late-onset AD is shaped by complex processes, including aging, genetic risks, life styles, and numerous factors inside and outside the brain [6, 7]. We have so far focused on investigating the neuronal intrinsic effects of human tau in the absence of non-autonomous response. Neuroinflammation represents a hallmark of AD and contributes significantly to the disease pathogenesis. We plan to develop *in vivo* tauopathy models using the same set of AAV vectors to dissect the interaction between hTau<sup>+</sup> neurons and glial populations known to play critical roles in tau-induced neurodegeneration [81, 82]. Another limitation is that we have only characterized the longest 2N4R form so far, but both 3R and 4R tau isoforms are implicated in AD [5]. Thus, future studies are necessary to elucidate the role played by different tau isoforms. In AD, tau pathology develops progressively and follows a topological pattern, where regional vulnerability has been postulated [83, 84]. Hence, it would be important to further examine the regional response by neurons to non-mutated tau in detail.

**Supplementary Information** The online version contains supplementary material available at <https://doi.org/10.1007/s12035-023-03720-1>.

**Acknowledgments** We are grateful for the generosity of Drs. Sebastian Kügler and Fred Van Leuven for providing the AAV vectors containing human 2N4R tau, Dr. Peter Davies for providing CP13, PHF-1 and MC1 antibodies, and Dr. R. Kaye for advising tau oligomer detection. We thank Austin Seal at Gene Vector Core at Baylor College of Medicine for AAV packaging service. The schematic was created with BioRender.

**Authors' contributions** Conceptualization, W.C. and S.L.; methodology, S.L., E.R.R., and W.C.; formal analysis, S.L. and W.C.; investigation, S.L. and E.R.R.; writing – original draft, W.C. and S.L.; writing – review & editing, Y.W., E.R.R., T.W. and W.C.; visualization, S.L.; supervision, W.C.; project administration, W.C.; funding acquisition, W.C.. All authors read and approved the final manuscript.

**Funding** This study was supported by NIH grants AG057587, AG074283, DK122708-03S1, BrightFocus ADR A20183775, and Brown Foundation 2020 Healthy Aging Initiative (W.C.).

**Availability of supporting data** • RNAseq data has been deposited in GEO. Accession number 246259.

## Declarations

**Ethical approval and consent to participate** Not applicable.

**Consent for publication** Not applicable.

**Competing interests** Nothing to declare.

**Open Access** This article is licensed under a Creative Commons Attribution 4.0 International License, which permits use, sharing, adaptation, distribution and reproduction in any medium or format, as long as you give appropriate credit to the original author(s) and the source, provide a link to the Creative Commons licence, and indicate if changes were made. The images or other third party material in this article are included in the article's Creative Commons licence, unless indicated

otherwise in a credit line to the material. If material is not included in the article's Creative Commons licence and your intended use is not permitted by statutory regulation or exceeds the permitted use, you will need to obtain permission directly from the copyright holder. To view a copy of this licence, visit <http://creativecommons.org/licenses/by/4.0/>.

## References

- Josephs K, Current A (2017) Understanding of Neurodegenerative Diseases Associated With the Protein Tau. *Mayo Clinic proceedings Mayo Clinic* 92:1291–1303. <https://doi.org/10.1016/j.mayocp.2017.04.016>
- Samudra N, Lane-Donovan C, VandeVrede L, Boxer AL (2023) Tau pathology in neurodegenerative disease: disease mechanisms and therapeutic avenues. *J Clin Invest* 133. 10.1172/JCI168553
- Holtzman DM et al (2016) Tau: From research to clinical development. *Alzheimer's & Dementia J Alzheimer's Assoc* 12:1033–1039. <https://doi.org/10.1016/j.jalz.2016.03.018>
- Chang CW, Shao E, Mucke L (2021) Tau: Enabler of diverse brain disorders and target of rapidly evolving therapeutic strategies. *Science* 371:eabb8255. <https://doi.org/10.1126/science.abb8255>
- Wang Y, Mandelkow E (2016) Tau in physiology and pathology. *Nat Rev Neurosci* 17:5–21. <https://doi.org/10.1038/nrn.2015.1>
- Knopman DS et al (2021) Alzheimer disease. *Nat Rev Dis Primers* 7:33. <https://doi.org/10.1038/s41572-021-00269-y>
- Scheltens P et al (2021) Alzheimer's disease. *Lancet* 397:1577–1590. [https://doi.org/10.1016/S0140-6736\(20\)32205-4](https://doi.org/10.1016/S0140-6736(20)32205-4)
- Tracy TE, Gan L (2018) Tau-mediated synaptic and neuronal dysfunction in neurodegenerative disease. *Curr Opin Neurobiol* 51:134–138. <https://doi.org/10.1016/j.conb.2018.04.027>
- Guo T, Noble W, Hanger DP (2017) Roles of tau protein in health and disease. *Acta Neuropathol* 133:665–704. <https://doi.org/10.1007/s00401-017-1707-9>
- Goedert M, Jakes R (2005) Mutations causing neurodegenerative tauopathies. *Biochim Biophys Acta* 1739:240–250. <https://doi.org/10.1016/j.bbadis.2004.08.007>
- Dujardin S et al (2020) Tau molecular diversity contributes to clinical heterogeneity in Alzheimer's disease. *Nat Med* 26:1256–1263. <https://doi.org/10.1038/s41591-020-0938-9>
- Wesseling H et al. (2020) Tau PTM Profiles Identify Patient Heterogeneity and Stages of Alzheimer's Disease. *Cell* 183, 1699–1713 e1613. 10.1016/j.cell.2020.10.029
- Verheyen A et al (2015) Using Human iPSC-Derived Neurons to Model TAU Aggregation. *PLoS One* 10:e0146127. <https://doi.org/10.1371/journal.pone.0146127>
- Gotz J et al (2004) Transgenic animal models of Alzheimer's disease and related disorders: histopathology, behavior and therapy. *Mol Psychiatry* 9:664–683. <https://doi.org/10.1038/sj.mp.4001508>
- Gotz J (2001) Tau and transgenic animal models. *Brain Res Brain Res Rev* 35:266–286. [https://doi.org/10.1016/s0165-0173\(01\)00055-8](https://doi.org/10.1016/s0165-0173(01)00055-8)
- Jankowsky JL, Zheng H (2017) Practical considerations for choosing a mouse model of Alzheimer's disease. *Mol Neurodegener* 12:89. <https://doi.org/10.1186/s13024-017-0231-7>
- Croft CL et al (2019) rAAV-based brain slice culture models of Alzheimer's and Parkinson's disease inclusion pathologies. *J Exp Med* 216:539–555. <https://doi.org/10.1084/jem.20182184>
- Bucci M, Chiotis K (2021) Nordberg, A. & Alzheimer's Disease Neuroimaging, I. Alzheimer's disease profiled by fluid and imaging markers: tau PET best predicts cognitive decline. *Mol. Psychiatry* 26:5888–5898. <https://doi.org/10.1038/s41380-021-01263-2>



19. Aschenbrenner AJ, Gordon BA, Benzinger TLS, Morris JC, Hasenstab JJ (2018) Influence of tau PET, amyloid PET, and hippocampal volume on cognition in Alzheimer disease. *Neurology* 91:e859–e866. <https://doi.org/10.1212/WNL.0000000000006075>
20. Tracy TE et al. (2022) Tau interactome maps synaptic and mitochondrial processes associated with neurodegeneration. *Cell* 185, 712–728 e714. [10.1016/j.cell.2021.12.041](https://doi.org/10.1016/j.cell.2021.12.041)
21. Montalbano M et al (2021) Tau Modulates mRNA Transcription, Alternative Polyadenylation Profiles of hnRNPs, Chromatin Remodeling and Spliceosome Complexes. *Front Mol Neurosci* 14:742790. <https://doi.org/10.3389/fnmol.2021.742790>
22. Holmes BB et al (2014) Proteopathic tau seeding predicts tauopathy in vivo. *Proc Natl Acad Sci U S A* 111:E4376–E4385. <https://doi.org/10.1073/pnas.1411649111>
23. Bell M, Zempel H (2022) SH-SY5Y-derived neurons: a human neuronal model system for investigating TAU sorting and neuronal subtype-specific TAU vulnerability. *Rev Neurosci* 33:1–15. <https://doi.org/10.1515/revneuro-2020-0152>
24. Garcia-Leon JA et al (2018) Generation of a human induced pluripotent stem cell-based model for tauopathies combining three microtubule-associated protein TAU mutations which displays several phenotypes linked to neurodegeneration. *Alzheimer's & Dementia J Alzheimer's Assoc* 14:1261–1280. <https://doi.org/10.1016/j.jalz.2018.05.007>
25. Jaworski T et al (2009) AAV-tau mediates pyramidal neurodegeneration by cell-cycle re-entry without neurofibrillary tangle formation in wild-type mice. *PLoS One* 4:e7280. <https://doi.org/10.1371/journal.pone.0007280>
26. Roy ER et al. (2022) Concerted type I interferon signaling in microglia and neural cells promotes memory impairment associated with amyloid beta plaques. *Immunity* 55, 879–894 e876. [10.1016/j.immuni.2022.03.018](https://doi.org/10.1016/j.immuni.2022.03.018)
27. Farmer KM et al (2020) P53 aggregation, interactions with tau, and impaired DNA damage response in Alzheimer's disease. *Acta Neuropathologica Commun* 8:132. <https://doi.org/10.1186/s40478-020-01012-6>
28. Behl C (2000) Apoptosis and Alzheimer's disease. *J Neural Transm (Vienna)* 107:1325–1344. <https://doi.org/10.1007/s007020070021>
29. Porter AG, Janicke RU (1999) Emerging roles of caspase-3 in apoptosis. *Cell Death Differ* 6:99–104. <https://doi.org/10.1038/sj.cdd.4400476>
30. Nakano K, Vousden KH (2001) PUMA, a novel proapoptotic gene, is induced by p53. *Mol Cell* 7:683–694. [https://doi.org/10.1016/s1097-2765\(01\)00214-3](https://doi.org/10.1016/s1097-2765(01)00214-3)
31. Mekhail K, Moazed D (2010) The nuclear envelope in genome organization, expression and stability. *Nat Rev Mol Cell Biol* 11:317–328. <https://doi.org/10.1038/nrm2894>
32. Mah LJ (2010) El-Osta, A. & Karagiannis, T. C. gammaH2AX: a sensitive molecular marker of DNA damage and repair. *Leukemia* 24:679–686. <https://doi.org/10.1038/leu.2010.6>
33. Fridman JS, Lowe SW (2003) Control of apoptosis by p53. *Oncogene* 22:9030–9040. <https://doi.org/10.1038/sj.onc.1207116>
34. Zhou BB, Elledge SJ (2000) The DNA damage response: putting checkpoints in perspective. *Nature* 408:433–439. <https://doi.org/10.1038/35044005>
35. Bohmann D et al (1987) Human proto-oncogene c-jun encodes a DNA binding protein with structural and functional properties of transcription factor AP-1. *Science* 238:1386–1392. <https://doi.org/10.1126/science.2825349>
36. Yarza R, Vela S, Solas M, Ramirez MJ (2015) c-Jun N-terminal Kinase (JNK) Signaling as a Therapeutic Target for Alzheimer's Disease. *Front Pharmacol* 6:321. <https://doi.org/10.3389/fphar.2015.00321>
37. Watkins TA et al (2013) DLK initiates a transcriptional program that couples apoptotic and regenerative responses to axonal injury. *Proc Natl Acad Sci U S A* 110:4039–4044. <https://doi.org/10.1073/pnas.1211074110>
38. Welsbie DS et al (2019) Targeted disruption of dual leucine zipper kinase and leucine zipper kinase promotes neuronal survival in a model of diffuse traumatic brain injury. *Mol Neurodegener* 14:44. <https://doi.org/10.1186/s13024-019-0345-1>
39. Welsbie DS et al (2013) Functional genomic screening identifies dual leucine zipper kinase as a key mediator of retinal ganglion cell death. *Proc Natl Acad Sci U S A* 110:4045–4050. <https://doi.org/10.1073/pnas.1211284110>
40. Gerdt J, Summers DW, Milbrandt J, DiAntonio A (2016) Axon Self-Destruction: New Links among SARM1, MAPKs, and NAD+ Metabolism. *Neuron* 89:449–460. <https://doi.org/10.1016/j.neuron.2015.12.023>
41. Le Pichon CE et al (2017) Loss of dual leucine zipper kinase signaling is protective in animal models of neurodegenerative disease. *Sci Transl Med* 9:eag0394. <https://doi.org/10.1126/scitranslmed.aag0394>
42. Fulga TA et al (2007) Abnormal bundling and accumulation of F-actin mediates tau-induced neuronal degeneration in vivo. *Nat Cell Biol* 9:139–148. <https://doi.org/10.1038/ncb1528>
43. Hong M et al (1998) Mutation-specific functional impairments in distinct tau isoforms of hereditary FTDP-17. *Science* 282:1914–1917. <https://doi.org/10.1126/science.282.5395.1914>
44. Margolis RL, Wilson L (1977) Addition of colchicine--tubulin complex to microtubule ends: the mechanism of substoichiometric colchicine poisoning. *Proc Natl Acad Sci U S A* 74:3466–3470. <https://doi.org/10.1073/pnas.74.8.3466>
45. Valakh V, Frey E, Babetto E, Walker LJ, DiAntonio A (2015) Cytoskeletal disruption activates the DLK/JNK pathway, which promotes axonal regeneration and mimics a preconditioning injury. *Neurobiol Dis* 77:13–25. <https://doi.org/10.1016/j.nbd.2015.02.014>
46. Gamache JE et al (2020) Developmental Pathogenicity of 4-Repeat Human Tau Is Lost with the P301L Mutation in Genetically Matched Tau-Transgenic Mice. *J Neurosci* 40:220–236. <https://doi.org/10.1523/JNEUROSCI.1256-19.2019>
47. Shi Y et al (2021) Structure-based classification of tauopathies. *Nature* 598:359–363. <https://doi.org/10.1038/s41586-021-03911-7>
48. Saint-Aubert L et al (2017) Tau PET imaging: present and future directions. *Mol Neurodegener* 12:19. <https://doi.org/10.1186/s13024-017-0162-3>
49. Wang X et al (2019) Tau interactome analyses in CRISPR-Cas9 engineered neuronal cells reveal ATPase-dependent binding of wild-type but not P301L Tau to non-muscle myosins. *Sci Rep* 9:16238. <https://doi.org/10.1038/s41598-019-52543-5>
50. Bhaskar K, Yen SH, Lee G (2005) Disease-related modifications in tau affect the interaction between Fyn and Tau. *J Biol Chem* 280:35119–35125. <https://doi.org/10.1074/jbc.M505895200>
51. Coppede F, Migliore L (2015) DNA damage in neurodegenerative diseases. *Mutat Res* 776:84–97. <https://doi.org/10.1016/j.mrfmmm.2014.11.010>
52. Stein D, Toiber D (2017) DNA damage and neurodegeneration: the unusual suspect. *Neural Regen Res* 12:1441–1442. <https://doi.org/10.4103/1673-5374.215254>
53. Jeppesen DK, Bohr VA, Stevnsner T (2011) DNA repair deficiency in neurodegeneration. *Prog Neurobiol* 94:166–200. <https://doi.org/10.1016/j.pneurobio.2011.04.013>
54. Andorfer C et al (2005) Cell-cycle reentry and cell death in transgenic mice expressing nonmutant human tau isoforms. *J Neurosci* 25:5446–5454. <https://doi.org/10.1523/JNEUROSCI.4637-04.2005>
55. Rossi G et al (2008) A new function of microtubule-associated protein tau: involvement in chromosome stability. *Cell Cycle* 7:1788–1794. <https://doi.org/10.4161/cc.7.12.6012>

56. Shanbhag NM et al (2019) Early neuronal accumulation of DNA double strand breaks in Alzheimer's disease. *Acta Neuropathologica Commun* 7:77. <https://doi.org/10.1186/s40478-019-0723-5>
57. Simpson JE et al (2015) A neuronal DNA damage response is detected at the earliest stages of Alzheimer's neuropathology and correlates with cognitive impairment in the Medical Research Council's Cognitive Function and Ageing Study ageing brain cohort. *Neuropathol Appl Neurobiol* 41:483–496. <https://doi.org/10.1111/nan.12202>
58. Bukar Maina M, Al-Hilaly YK, Serpell LC (2016) Nuclear Tau and Its Potential Role in Alzheimer's Disease. *Biomolecules* 6:9. <https://doi.org/10.3390/biom6010009>
59. Coyne AN, Rothstein JD (2022) Nuclear pore complexes - a doorway to neural injury in neurodegeneration. *Nature reviews. Neurology* 18:348–362. <https://doi.org/10.1038/s41582-022-00653-6>
60. Prissette M et al (2022) Disruption of nuclear envelope integrity as a possible initiating event in tauopathies. *Cell Rep* 40:111249. <https://doi.org/10.1016/j.celrep.2022.111249>
61. Eftekharzadeh B et al. (2018) Tau Protein Disrupts Nucleocytoplasmic Transport in Alzheimer's Disease. *Neuron* 99, 925–940 e927. [10.1016/j.neuron.2018.07.039](https://doi.org/10.1016/j.neuron.2018.07.039)
62. Frost B, Bardai FH, Feany MB (2016) Lamin Dysfunction Mediates Neurodegeneration in Tauopathies. *Curr Biol* 26:129–136. <https://doi.org/10.1016/j.cub.2015.11.039>
63. Frost B, Hemberg M, Lewis J, Feany MB (2014) Tau promotes neurodegeneration through global chromatin relaxation. *Nat Neurosci* 17:357–366. <https://doi.org/10.1038/nn.3639>
64. Gonzalo S in *Cancer Biology and the Nuclear Envelope: Recent Advances May Elucidate Past Paradoxes* (eds Eric C. Schirmer & Jose I. de las Heras) 377–399 (Springer New York, 2014).
65. Asada-Utsugi M et al (2022) Failure of DNA double-strand break repair by tau mediates Alzheimer's disease pathology in vitro. *Commun Biol* 5:358. <https://doi.org/10.1038/s42003-022-03312-0>
66. Cimini S et al (2022) P301L tau mutation leads to alterations of cell cycle, DNA damage response and apoptosis: Evidence for a role of tau in cancer. *Biochem Pharmacol* 200:115043. <https://doi.org/10.1016/j.bcp.2022.115043>
67. Norbury CJ, Zhivotovsky B (2004) DNA damage-induced apoptosis. *Oncogene* 23:2797–2808. <https://doi.org/10.1038/sj.onc.1207532>
68. Fricker M, Tolkovsky AM, Borutaite V, Coleman M, Brown GC (2018) Neuronal Cell Death *Physiol Rev* 98:813–880. <https://doi.org/10.1152/physrev.00011.2017>
69. Farley MM, Watkins TA (2018) Intrinsic Neuronal Stress Response Pathways in Injury and Disease. *Annu Rev Pathol* 13:93–116. <https://doi.org/10.1146/annurev-pathol-012414-040354>
70. Coleman M (2005) Axon degeneration mechanisms: commonality amid diversity. *Nat Rev Neurosci* 6:889–898. <https://doi.org/10.1038/nrn1788>
71. Ishihara T et al (1999) Age-dependent emergence and progression of a tauopathy in transgenic mice overexpressing the shortest human tau isoform. *Neuron* 24:751–762. [https://doi.org/10.1016/s0896-6273\(00\)81127-7](https://doi.org/10.1016/s0896-6273(00)81127-7)
72. Spittaels K et al (1999) Prominent axonopathy in the brain and spinal cord of transgenic mice overexpressing four-repeat human tau protein. *Am J Pathol* 155:2153–2165. [https://doi.org/10.1016/S0002-9440\(10\)65533-2](https://doi.org/10.1016/S0002-9440(10)65533-2)
73. Terwel D et al (2005) Changed conformation of mutant Tau-P301L underlies the moribund tauopathy, absent in progressive, nonlethal axonopathy of Tau-4R/2N transgenic mice. *J Biol Chem* 280:3963–3973. <https://doi.org/10.1074/jbc.M409876200>
74. Probst A et al (2000) Axonopathy and amyotrophy in mice transgenic for human four-repeat tau protein. *Acta Neuropathol* 99:469–481. <https://doi.org/10.1007/s004010051148>
75. Ghosh AS et al (2011) DLK induces developmental neuronal degeneration via selective regulation of proapoptotic JNK activity. *J Cell Biol* 194:751–764. <https://doi.org/10.1083/jcb.201103153>
76. Stokin GB et al (2005) Axonopathy and transport deficits early in the pathogenesis of Alzheimer's disease. *Science* 307:1282–1288. <https://doi.org/10.1126/science.1105681>
77. Su JH, Cummings BJ, Cotman CW (1993) Identification and distribution of axonal dystrophic neurites in Alzheimer's disease. *Brain Res* 625:228–237. [https://doi.org/10.1016/0006-8993\(93\)91063-x](https://doi.org/10.1016/0006-8993(93)91063-x)
78. Gibson PH (1987) Ultrastructural abnormalities in the cerebral neocortex and hippocampus associated with Alzheimer's disease and aging. *Acta Neuropathol* 73:86–91. <https://doi.org/10.1007/BF00695506>
79. Johnson ECB et al (2022) Large-scale deep multi-layer analysis of Alzheimer's disease brain reveals strong proteomic disease-related changes not observed at the RNA level. *Nat Neurosci* 25:213–225. <https://doi.org/10.1038/s41593-021-00999-y>
80. Swarup V et al (2020) Identification of Conserved Proteomic Networks in Neurodegenerative Dementia. *Cell Rep* 31:107807. <https://doi.org/10.1016/j.celrep.2020.107807>
81. Wang C et al. (2021) Selective removal of astrocytic APOE4 strongly protects against tau-mediated neurodegeneration and decreases synaptic phagocytosis by microglia. *Neuron* 109, 1657–1674 e1657. [10.1016/j.neuron.2021.03.024](https://doi.org/10.1016/j.neuron.2021.03.024)
82. Shi Y et al (2017) ApoE4 markedly exacerbates tau-mediated neurodegeneration in a mouse model of tauopathy. *Nature* 549:523–527. <https://doi.org/10.1038/nature24016>
83. Fu H et al (2019) A tau homeostasis signature is linked with the cellular and regional vulnerability of excitatory neurons to tau pathology. *Nat Neurosci* 22:47–56. <https://doi.org/10.1038/s41593-018-0298-7>
84. van der Kant R, Goldstein LSB, Ossenkoppele R (2020) Amyloid-beta-independent regulators of tau pathology in Alzheimer disease. *Nat Rev Neurosci* 21:21–35. <https://doi.org/10.1038/s41583-019-0240-3>

**Publisher's Note** Springer Nature remains neutral with regard to jurisdictional claims in published maps and institutional affiliations.